Chapter 6

Light-Weight Flexible Solid-State Supercapacitor Based on Highly Crystalline 2-D BiOCl Nanoplates/ MWCNT Nanocomposites

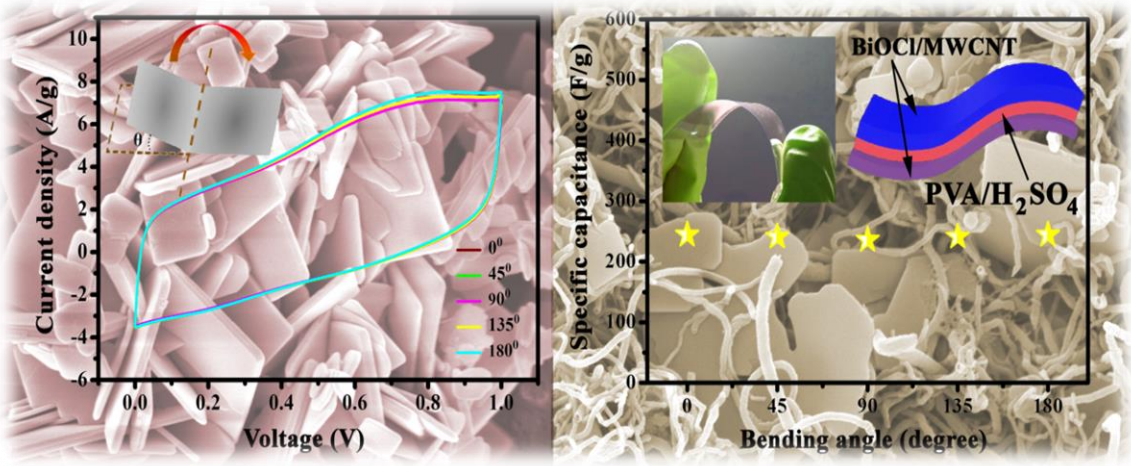

Work presented in this chapter has been published in:

J.Alloys Compd. 820 (2020) 153115

Shibsankar Dutta*, *Debopriya Shikder, Shreyasi Pal and Sukanta De

6.1. Introduction

Multi-electron transfer properties of Bismuth oxides and Bismuth oxyhalides during electrochemical reaction make them attractive candidates for supercapacitor application. Nano sheets, nano belts and different nano structures of bismuth oxides based supercapacitor were reported which exhibiting specific capacitances between 98~996 F/g. Bi_2O_3 film grown on copper substrates using electroplating as supercapacitor electrode was first reported by Gujar and his co-worker.[5] Asymmetric supercapacitor based on (+ electrode) MnO_2//(- electrode)β-Bi_2O_3 was reported by Ma et al , which obtained high energy density of 32.4Wh/ kg.[6] Bismuth oxychloride (BiOCl) another member of the same family have tetragonal lamellar structure, in which [Cl–Bi–O–Bi–Cl] sheets are stacked together by the van der Waals interaction through the Cl atoms along the c-axis. Until now, different morphologies of BiOCl materials by several synthesis procedures were reported.[7-13] Among different morphologies two-dimensional BiOCl nanoplate has shown potential applications in photocatalytic, optical, electrical and biomedical grounds because of its perfect crystallinity, geometric anisotropy, excellent photostability, electronic properties and nontoxicity. Wang et.al reported one-pot strategy for the synthesis of uniform PANi thorn/BiOCl chip (BPB) heterostructures at a low temperature using Bi_2S_3 nanowires and that BPB-modified electrode exhibited an specific capacitance of 169.9 F/ g at 0.5 A/ g. One dimensional polyaniline thorn/BiOCl chip heterostructures: self-sacrificial template-induced synthesis and electrochemical performance.[14] Liu and his co-worker reported AC/BiOCl asymmetric supercapacitor, exhibits a maximum capacitance value of 124 F/ g at 0.5 A/ g.[15] Q.X. Xia et al. reported a bismuth oxychloride nanosheets-immobilised $Ti_3C_2T_x$ MXene material (TCBOC) electrode with specific capacitance 247.8 F/g at the current density of 1 A/g.[16] Nevertheless, to the best of our knowledge, except these few reports there is no other report on BiOCl as supecapacitor electrode.

Here, we have adopted a simple, cost-effective hydrothermal approach for the synthesis of scalable amount of 2D bismuth oxychloride (BiOCl) nanoplates. Thin flexible films of BiOCl/MWCNT composites have been prepared with varying the weight percentage. A remarkable electrochemical performance has been obtained for BiOCl/MWCNT flexible solid state symmetric supercapacitor (FSSSC) with PVA/H_2SO_4 gel as solid electrolyte. Among various compositions, 60% BiOCl loaded electrodes ($FSSC_{60}$) delivers a highest specific capacitance of 421F/g at 5mV/s. Furthermore, $FSSSC_{60}$

exhibits a high energy density of 14.62 Wh/kg at power density 947.5 W/kg. The $FSSSC_{60}$ shows excellent durability with 94 % of initial specific capacitance after 2000 cycles. In addition, as fabricated device exhibits good flexibility and retains almost constant performance after bending through different angles.

6.2. Experimental

6.2.1.Materials:

Bismuth nitrate [$Bi(NO_3)_3 \cdot 5H_2O$], potassium chloride (KCl) sodium hydroxide (NaOH), sodium dodecyl sulfate (SDS, >90%), sulphuric acid (H_2SO_4, 98%), polyvinyal alcohol (PVA) were purchased from Merck Specialties Pvt. Ltd. Multiwall carbon nanotube (OD: 60-100 nm, L: 5-15nm) was purchased from io-Il-Tech nanomateials. All chemicals were used without further purification.

6.2.2. Synthesis of BiOCl nano-plate:

The plate-like BiOCl was synthesized according to the procedure described in the previously reported literature.[17] In detail, 2 mmol of $Bi(NO_3)_3 \cdot 5H_2O$ and 2 mmol of KCl were successively dissolved into 30 mL of deionized water under magnetic stirring at room temperature, Subsequently, pH value of solution was adjusted to about 6.0 by adding 1M NaOH solution. After continuously stirring for 30 min, mixture solution was transferred into 50 mL Teflon-lined stainless steel autoclave and allowed to be heated at 160 °C for 24 h in a static state. After that allowed it to air cooled to room temperature. The resulting white particles were collected and successively washed with ethanol and deionized water and finally dried at 60 °C in air.

6.2.3. Preparation of CNT dispersions:

Firstly, stock solutions of sodium dodecylsulphate (SDS) of concentration 5mg/ml in deionized water was prepared by overnight magnetic stirring at room temperature. Subsequently, carbon nanotube dispersions were prepared using SDS solutions with surfactant, CNT mass ratio 5:1, under high power ultrasonic irradiation for 5 minutes followed by low power sonic bath treatment for 1 hour. Finally, dispersions were subjected for another 5 minutes high power ultrasonic irradiation treatment. After overnight rest, dispersions were centrifuged at 5500 rpm for 90 minutes. Lastly, for future application supernatant was carefully decanted.[18] We have followed this method to disperse both SWCNT and MWCNT.

6.2.4. Electrode preparation:

BiOCl nano-plates of concentration 1mg/ml were dispersed in ethanol by low power ultrasonic bath sonication for 5 minutes. Subsequently, prepared MWCNT dispersions and BiOCl dispersions were mixed together with different weight percentages to make thin films on cellulose membranes with masking one portion using vacuum filtration. After complete filtration, the film was allowed to dry on filter membrane keeping the filtration setup intact. We have removed the mask before depositing SWCNT thin film on top of BiOCl/MWCNT film under vacuum filtration condition and washed with DI water several times (as shown in the fig.1). Then thin films were transfer on flexible PET substrate as reported in the literature.[19]

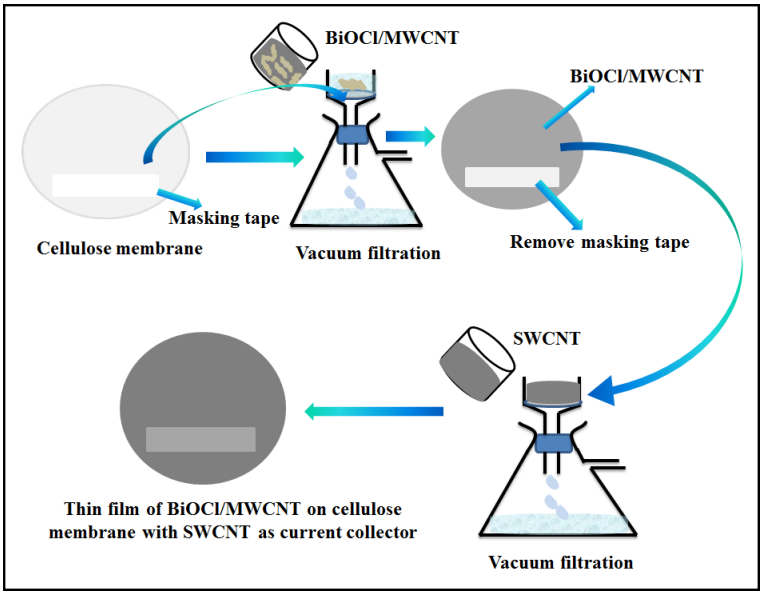

Figure 6.1. Thin film Preparation using vacuum filtration

6.2.5. Fabrication of flexible symmetric solid state supercapacitor (FSSSC):

BiOCl/MWCNT thin films on flexible PET substrates were used as both positive and negative electrode, whereas PVA/H_2SO_4 gel sandwiched between the electrodes acted as solid electrolyte of FSSSC (fig.6.2) where SWCNT network in between PET and composite thin film act as current collectors. Henceforth, We designate the solid state supercapacitors with loading 100 wt%, 75 wt%, 60 wt %, 50 wt %, 25 wt % and 0 wt% BiOCl as $FSSSC_{100}$, $FSSSC_{75}$, $FSSSC_{60}$, $FSSSC_{50}$, $FSSSC_{25}$ and $FSSSC_0$ respectively.

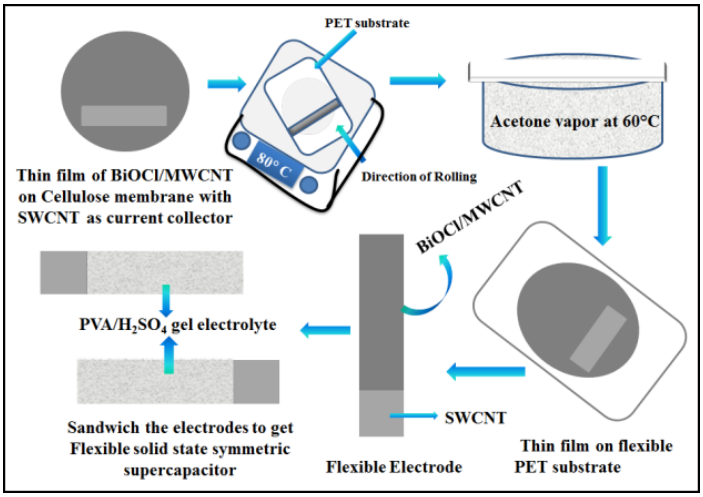

Figure 6.2. Fabrication of Flexible solid state supercapacitor

5.3. Characterization

Scanning electron microscope (SEM) images were taken by a FEI, MERLIN (Carl Zeiss) Scanning Electron Microscope. The Brunauer–Emmett–Teller (BET) and pore size distribution of samples were determined by Autosorb iQ Station 1 instrument using liquid nitrogen at 77 K based on the nitrogen adsorption-desorption isotherm. Transmission electron microscope (TEM) images of BiOCl were taken by JEM 2100 at an accelerating voltage of 200 keV. The structure of BiOCl and composite were examined by Rigaku-Ultima III X-ray diffractometer with CuKα radiation (l = 1.5418 Å) X-ray diffraction (XRD-6000) with Cu Kα radiation operating at 40kV, 60mA. Raman spectra were done with IHR550 spectrometer and a laser excitation wavelength of 532 nm. The electrochemical performance of BiOCl nano-plate and BiOCl/MWCNT were measured using two electrode system operated at CHI660E electrochemical work station at room temperature. Cyclic voltammetry (CV) and galvanometric charging discharging (GCD) tests of supercapacitors were measured with the potential window 0V to 1V. Electrochemical impedance spectroscopies (EIS) of the electrodes were recorded between 0.01 Hz to 100 KHz.

6.4. Result and discussion

6.4.1. Structural & morphological analysis:

Plate-like morphology of as prepared BiOCl were observed under transmission electron microscopy (TEM) image shown in Figure 6.3a. The selected-area electron diffraction (SAED) pattern (inset of Fig.6.3c) corresponding to the nano plates indicated the single-crystalline nature. Notably the size of the obtained nano-plate is about 500 nm as shown in the fig 6.3(b). High-resolution TEM (HRTEM) image (Figure 6.3b) displays clear

and continuous lattice fringes having lattice spacing of 0.275nm along the (110) atomic planes respectively.[15,17] The selected-area electron diffraction (SAED) pattern of the nano-plate is shown in the inset of fig.6.3c and revels the angle between (110) and (200) plane is 45° which is well match to the theoretical value.[17]

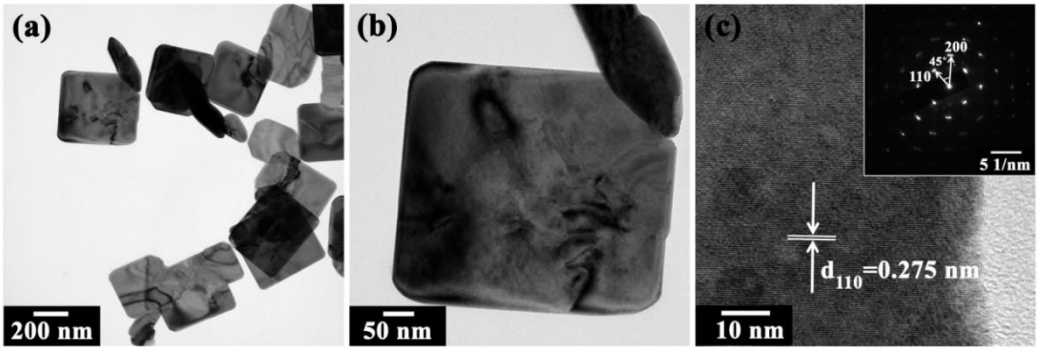

Figure.6.3 (a) TEM image of the BiOCl nanoplates (BC100:0), (b) TEM image of single BC100:0 nanoplate surface, (c) HRTEM image of the BC100:0 nanoplate surface and insert is the corresponding SAED pattern.

Fig 6.4(a) represent the schematic illustration of the crystal orientation of the BiOCl nanoplate whereas fig.6.4(b) shows the side and top view of the crystal structure.Fig.6.4(c) depicts the EDAX spectrum of BiOCl nanoplates conforming the presence Bi, O and Cl elements and their atomic % values are present in the table of fig.6.4(d) which indicates the atomic percentage ratio of Bi:O is 0.96 and O:Cl is 1.01 which are very close to 1.

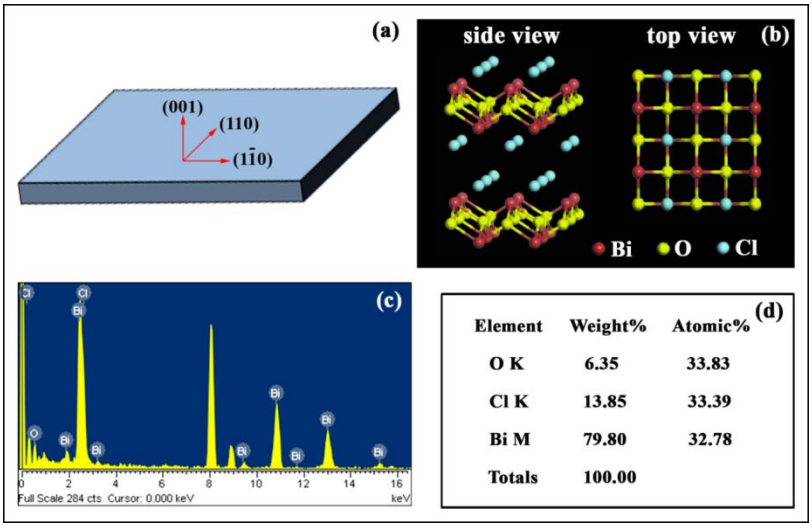

Figure.6.4. (a) Schematic illustration of the crystal orientation of the BiOCl nanoplate. (f) the crystal structure of BiOCl of the {001} facets; (c,d) EDX spectrum and corresponding atomic percentages of the BiOCl nanoplates (BC100:0).

The FESEM images reveals that the prepared samples consisted with 2 dimensional plate-like structures having size ~200-500 nm and thicknesses of 10-20 nm (Fig.6.5). The Fig 6.5(a-f) represents the FESEM images of the BiOCl/MWCNT composite thin films with different loading weight percentages of (100:0), (75:25), (60:40), (50:50), (25:75) and (0:100) respectively. we designate the samples corresponding to 100 Wt% of BiOCl, 75 Wt% of BiOCl, 60 Wt% of BiOCl, 50 Wt% of BiOCl, 25 Wt% of BiOCl and 0% of BiOCl as BC(100:0), BC(75:25), BC(60:40), BC(50:50), BC(25:75) and BC(0:100) respectively. The composite thin films exhibited an interconnected porous network, where MWCNTs were played the roles of the structural scaffolds. Further it is clearly visible that the most porous network was obtained for the (60:40) BiOCl/MWCNT composite, which explore more electro-active sites to the electrolyte ions and used for electrochemical studies.

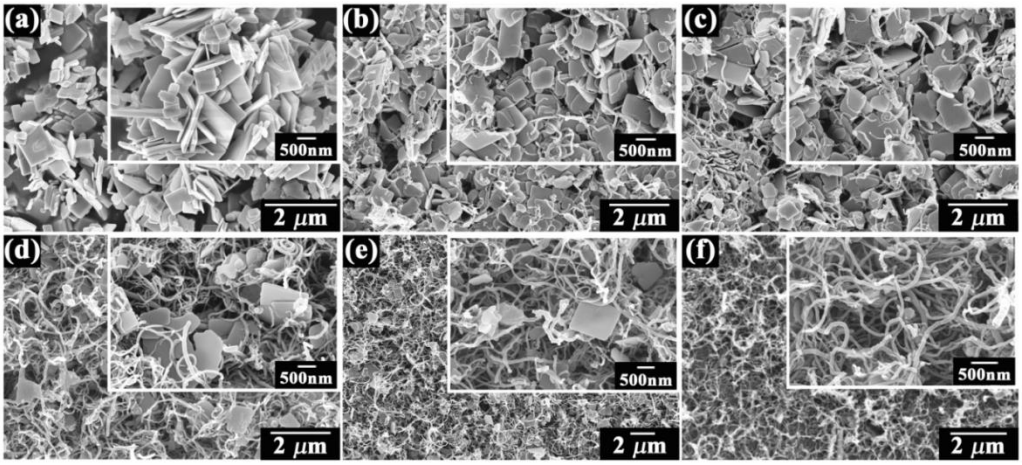

Figure.6.5. FESEM images of BiOCl nanoplates and BiOCl/MWCNT nanocomposites (a) BC100:0, (b) BC75:25, (c) BC60:40, (d) BC50:50, (e) BC25:75 and (f) BC0:100 respectively, Insets showing their high magnification images.

The crystallographic natures of the prepared samples were characterized by X-ray diffraction (XRD). Fig.6.6(a,(i)) shows the XRD pattern of the obtained BiOCl samples in the 2θ range from 10° to 80°. The observed diffraction peaks of the sample at 12°, 24°, 26°, 32°, 33°, 35°, 36°, 41°, 47°, 48°, 50°, 53°, 54°, 55°, 58°, 60°, 67°, 68°, 70°, 72°, 75°, 78° are assigned to the (001), (002), (101), (110), (102), (111), (003), (112), (200), (201), (113), (202), (211), (104), (212), (114), (220), (221), (204), (115), (214), (310) planes, which is well matched the reference BiOCl crystal structure (JCPDS No.06-0249). [15] The high diffraction peak ratio value of (101), (102) and (110) planes over the (001) plane suggests that the sample is preferentially grown along the

(101), (102), and (110) directions. Further no other impurity related peaks confirms the phase purity as well as the highly crystalline nature of the as-synthesized BiOCl samples. The XRD pattern of BiOCl/MWCNT (60:40) thin film (Fig.6.6 (a, ii) reveals that the diffraction peaks for MWCNT at 25.8° related to (002) plane overlapped with the peaks of BiOCl corresponding to 101 plane at 26°. All other diffraction peaks of BiOCl are presents in the XRD patterns of the composite.

Fig. 6.6(b) shows the Raman spectra of the sample. The peaks at 141 cm^{-1} is due the A1g stretching vibration of Bi-Cl. The peaks at 197 cm^{-1} is also assigned to the stretching vibration of Bi-Cl whereas peak at 396 cm^{-1} is attributed to the stretching vibration of Bi-O. [23,24] The Raman spectra of the composite(60wt% BiOCl and 40wt % of MWCNT) thin film depicts D and G peaks of MWCNT as well as peaks corresponding to BiOCl,[25] which conforms the presence of both MWCNT and BiOCl in the thin films, as shown in the Fig. 6.6(c).

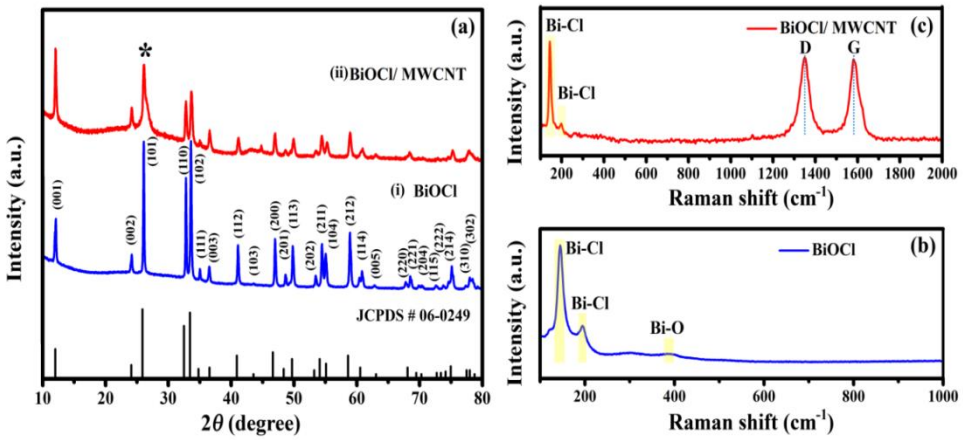

Figure.6.6. (a) XRD patterns and (b,c) Raman spectra of the BiOCl nanoplates (BC100:0) and BC60:40 BiOCl/MWCNT composites.

The chemical compositions and surface electronic state of the prepared BiOCl was investigated by X-ray photoelectron spectroscopy (XPS). The survey XPS Spectrum (Fig.6.7a) indicates the presence of Bi, O, Cl and C only. The signal at 284.48 eV is assigned to C1s, (Fig. 6.7b) which comes from the hydrocarbon of the XPS instrument itself.[26]. The two strong peaks at 165.2 eV (Bi4f5/2) and 159.9 eV (Bi4f7/2) in the Bi4f spectrum (Fig. 6.7c) are observed which indexed to the Bi^{3+} in BiOCl.[27,28] The peaks at 198.4 (Cl2p3/2) and 200 eV(Cl2p1/2) displayed in the Fig. 6.7d is the characteristic of Cl in BiOCl.[29] On the other hand the peak at 530.5 eV shown in the Fig. 6.7e was assigned to O1s of BiOCl.

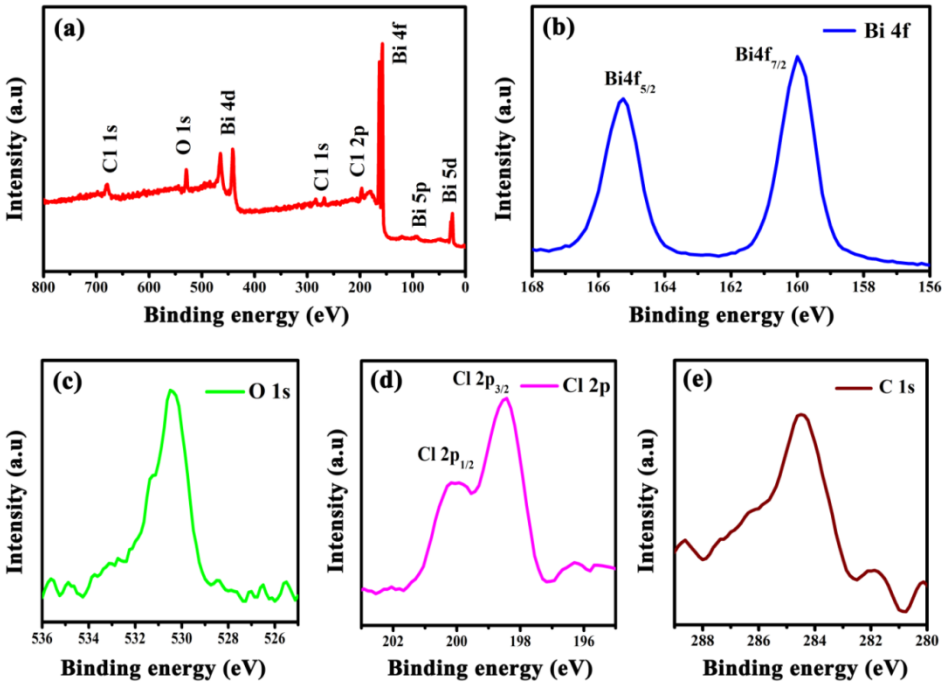

Figure 6.7. (a) XPS survey scan and XPS spectrum of the (b) Bi 4f, (c) O1s, (d) Cl 2p and (e) C 1s of the BC100:0 samples.

The N_2 adsorption–desorption measurement of the samples were done to obtain the textural parameters. The N_2 adsorption/desorption isotherms and corresponding pore size distribution curves (inset) of all the samples were shown in the figure 6.8(a)-(f). It can be observed that isotherms are of type-IV according to the IUPAC nomenclature and exhibit H3 hysteresis, which implies a mesoporous nature of the samples.[15]The specific surface area and pore size of the samples are presented in the table 6.1. From the bar diagram (Fig.6.9) it is evident that among the all sample BiOCl/ MWCNT (60/40) delivered more specific surface area as well as more pore volume and these results matching our FESEM results.

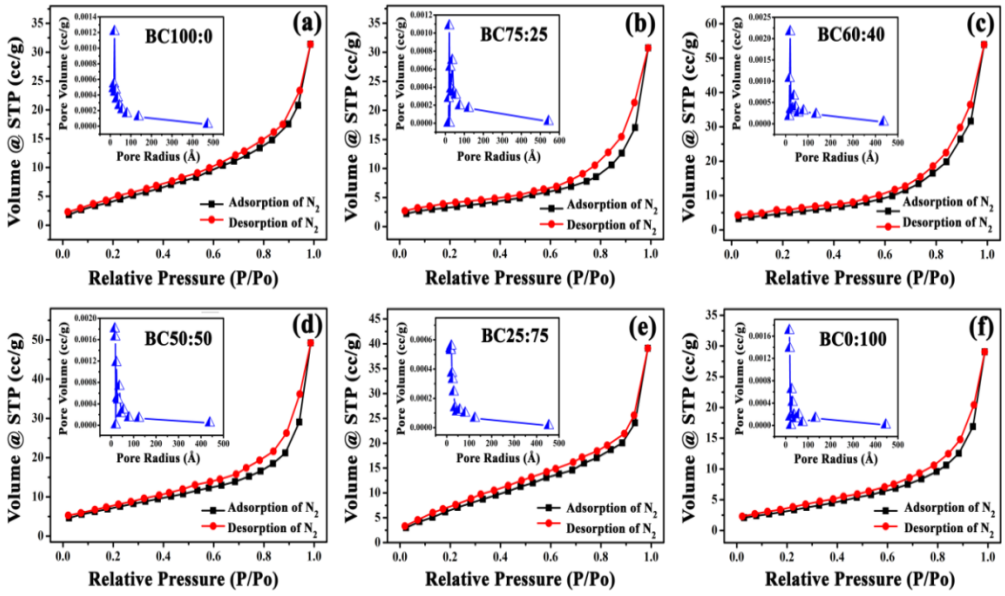

Figure 6.8. N_2 adsorption–desorption isotherms and corresponding BJH pore size distribution plots (inset fig) (a) BC100:0, (b) BC75:25, (c) BC60:40, (d) BC50:50, (e) BC25:75 and (f) BC0:100 respectively

Table 6.1. Textural parameters from BET analysis

Electrode Samples	Specific Surface Area (m^2/g)	Pore radius (Å)	Pore Volume (cc/g)
BC100	15.139	20.408	0.047
BC75	15.668	20.606	0.051
BC60	22.750	20.332	0.072
BC50	22.099	16.229	0.061
BC25	19.824	20.023	0.059
BC0	15.268	16.289	0.034

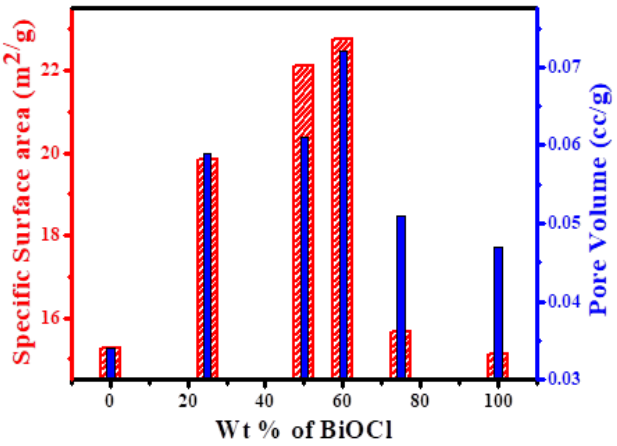

Figure6.9. Specific surface areas and pore volumes of all the samples from BET analysis. Specific surface areas and pore volumes of all the samples from BET analysis.

6.4.2. Electrochemical tests of the symmetric supercapacitor:

To investigate the electrochemical performance of the as-fabricated FSSSC device with different wt% of BiOCl/MWCNT loading, CV and GCD tests were carried out with potential window 0 V to 1 V at different scan rates and current densities respectively (Fig. 6.10 and 6.11).

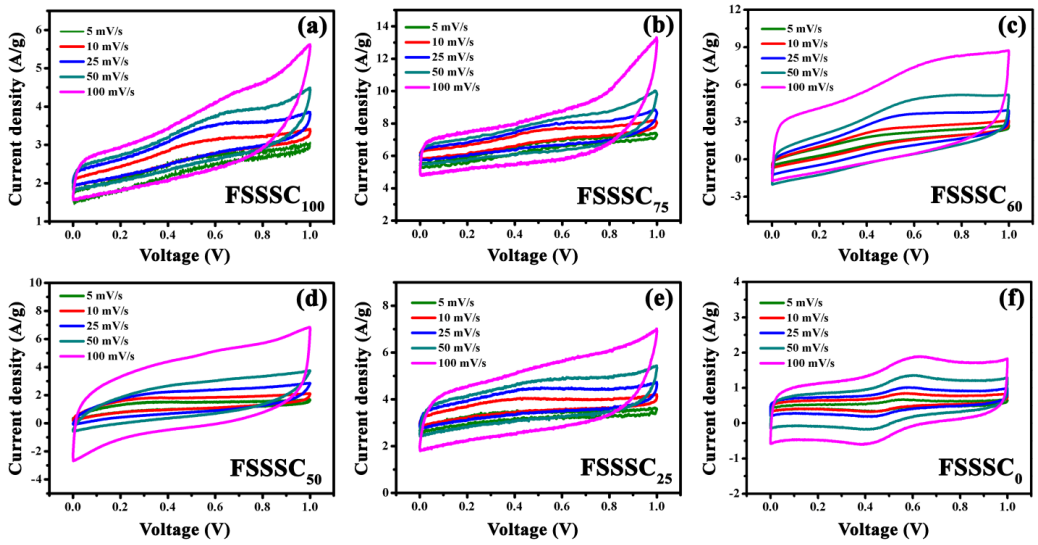

Figure 6.10. Cyclic voltammetry (CV) curves at different scan rates of (a) $FSSSC_{100}$, (b) $FSSSC_{75}$, (c) $FSSSC_{60}$, (d) $FSSSC_{50}$, (e) $FSSSC_{25}$ and (f) $FSSSC_{0}$ devices respectively.

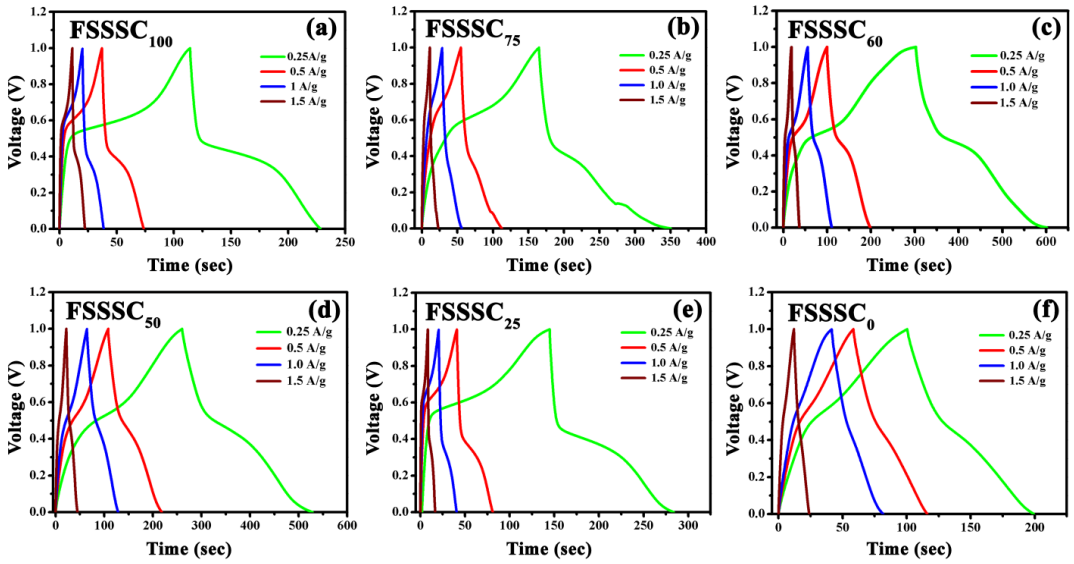

Figure 6.11. Galvanostatic charge discharge (GCD) curves at different current densities of SSC_{100} (a), SSC_{75} (b), SSC_{60} (c), SSC_{50} (d), SSC_{25} (e) and SSC_0 (f) devices respectively.

Fig 6.12(a) displays the GCD curves of all the FSSSC devices at current density 0.25 A/g, where the $FSSSC_{60}$ (60:40 BiOCl/MWCNT composite) gives the highest specific capacitance values. The specific capacitance values at 0.25A/g current density of the all FSSSC devices are calculated and the corresponding graph is shown in Fig 6.12b.

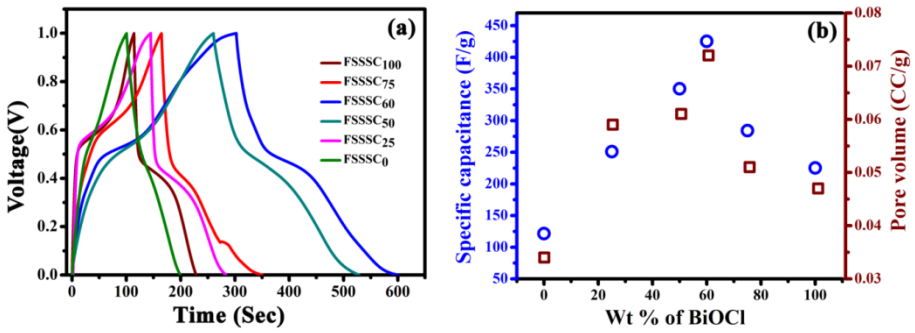

Figure 6.12. (a) GCD curves at a 0.25 A/g current density of all FSSSC (b) Specific capacitance and pore volume vs different wt% of BiOCl/MWCNT nano composites.

The superior electrochemical performance of $FSSSC_{60}$ amongst other different SSC can be attributed due to the best textural parameters (22.750 m^2/g surface area and 0.072 cc/g pore volume), obtained by BET analysis. The porous structure promotes electrolyte access and exposure the electro-active sites to the electrolyte. Also the conducting nature of MWCNT controls the fast charge transport. Thus we have picked 60:40(BiOCl/ MWCNT) composite electrode material for further electrochemical studies.

For further electrochemical study we have choose $FSSSC_{60}$ device. Fig.6.13 (a) and (b) shows the CV and GCD curves of $FSSSC_{60}$ at different scan rates and current density respectively. The obtained specific capacitance values from CV are 421F/g, 375 F/g, 323 F/g, 283 F/g, and 241 F/g at 5mv/s, 10 mV/s, 25 mV/s, 50 mV/s and 100 mV/s respectively. The redox reaction of H^+ ions with BiOCl can be described by the following reaction:

$$BiOCl + H_2O + 3e^- \rightarrow Bi + Cl^- + 2OH^-$$

$$2Bi + 6OH^- \leftrightarrow Bi_2O_3 + 3H_2O + 6e^-$$

Further we have measured the CV of $FSSSC_{60}$ by varying the voltage window for a fixed scan rate (100 mV/s) as shown in the fig.6.13(c). The CV curves maintain same nature at different potential windows, which indicates the stability of the supercapacitor.$FSSSC_{60}$ supercapacitor also shows outstanding stability after 2000 cycles, shown in the fig.6.13(d). The $FSSSC_{60}$ supercapacitor retains its 94% initial capacitance after 2000 cycles. The $FSSSC_{60}$ supercapacitor exhibits high energy density 14.62 Wh/kg at power density 947.5 W/kg. The Ragone plot of the as prepared $FSSSC_{60}$ and the previously reported symmetric and asymmetric supercapacitors is displayed in the Fig. 6.13(e).[15, 16, 30-37] We also studied electrochemical impedance spectroscopy tests to evaluate the capacitive behaviour of FSSSC60 Supercapacitor systematically. Fig. 6.13(f) shows Nyquist plots of electrodes over the frequency range of 0.01Hz 100 kHz. The corresponding equivalent circuit is shown in lower inset of Fig 6.13(e), which consists of a series and parallel combination of resistances, Rs, Rct (charge transfer resistance), CPE (constant phase element), and Zw (Warburg impedance).[35] The equivalent series resistance (ESR) values (Rs) is 3.94 Ω for SSC60. At lower frequency region in the Nyquist plot, the greater slope of the straight line indicates good capacitive behaviour of the sample, which also be conformed from the bode plot upper inset of Fig.6.13(e) where low frequency region phase angle closer to 65°.

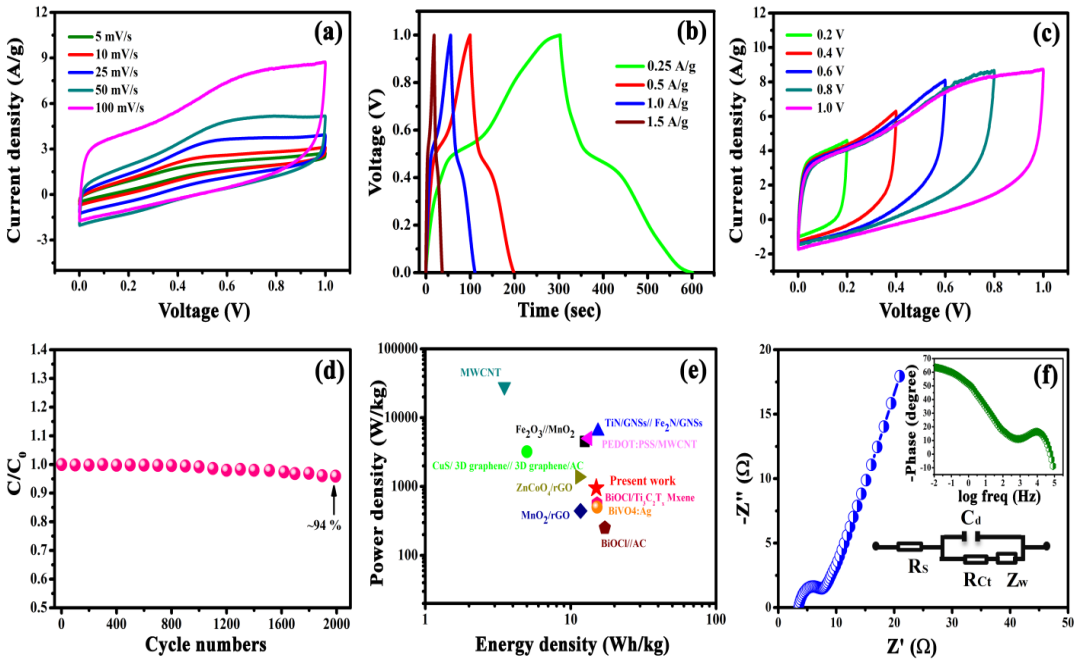

Figure 6.13.(a) CV curves of $FSSSC_{60}$ at different scan rates.(b) GCD curves of $FSSSC_{60}$ at different current densities, (c) CV curves of $FSSSC_{60}$ at 100mV/s scan rate for different voltage windows,(d)Cycle stability curve of $FSSSC_{60}$ at 100 mV/s, (e) Ragone plot for $FSSSC_{60}$, (e) Nyquist plots of $FSSSC_{60}$ and lower and upper inset shows equivalent circuit, and Bode plot of $FSSSC_{60}$ respectively.

Flexibility is fast becoming an exclusive feature in modern electronic devices. To this end, we have investigated the performance of our devices under a variety of bending conditions. We have done cyclic voltammetry study (at 100 mV/s) for the device $FSSSC_{60}$ at different bending angle and no significant changes in CV curves were observed as shown in the fig.6.14 (a) and schematic of bending angle is shown in inset of fig. 12(a). The corresponding specific capacitance value was almost remaining same during different bending angle, which is displayed in the fig 6.14(b), inset of the fig 6.14(b) displayed flexible thin film of BiOCl/MWCNT on a PET substrate.

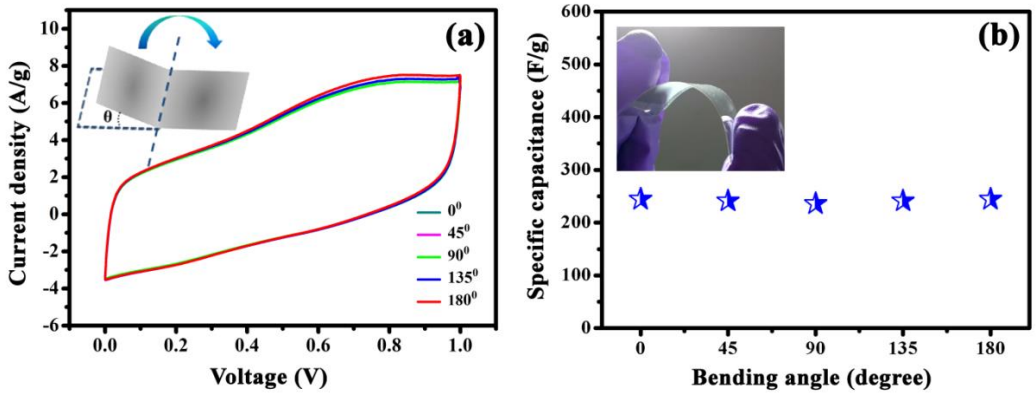

Figure 6.14.(a) Cyclic voltammetry curves at different bending conditions for $FSSSC_{60}$ at 100 mv/s scan rate, inset shows schematic diagram of bending angle, (b) Specific capacitance vs bending angle graph of $FSSSC_{60}$ and flexible electrode(inset fig).

6.5 Summary

In summary, we have fabricated 2D-BiOCl nanoplates / MWCNT nanocomposites based thin flexible supercapacitor with high specific capacitance and energy density and have been reported for the first time. Among different compositions, composite with 60 wt% exhibits highest specific capacitance of 421F/g and energy density 14.62 Wh/Kg. Variation in the electrochemical performance of BiOCl/MWCNT composites with different wt% is perfectly correlated with specific surface area and the pore size of composites. Excellent cycle stability with only 6% reduction in specific capacitance after 2000 cycles and good stability under bending, making the fabricated supercapacitor extremely promising as a flexible energy storage device.

6.6 References

1) L. Li, Z. A. Hu, N. An, Y. Y. Yang, Z. M. Li and H. Y. Wu, *J. Phys. Chem. C.* 2014**, 118**, 22865-22872.
2) J. Jiang, Y. Li, J. Liu, X. Huang, C. Yuan and X. W. Lou, *Adv.Mater.* 2012, **24**, 5166–5180.
3) I.K. Chakraborty, N. Chakrabarty, A. Senapati and A.K. Chakraborty, *J.Phys. Chem. C* 2018, **122**, 27180-27190.
4) S. Pal, S. Majumder, S. Dutta, S. Banerjee, B. Satpati and S. De, *J. Phys. D: Appl. Phys.* 2018, **51**, 375501.
5) P. Gujar, V.R. Shinde, C.D. Lokhande and S.H. Han, *J. Power Sources.* 2006, **161,** 1479–1485.

6) X.J. Ma, W.B. Zhang, L.B. Kong, Y.C. Luo and L. Kang, *Electrochim. Acta.* 2016, **192**, 45–51.
7) S. Jiang, X. Peng, Y. Hu and Z. Gui, *Mater. Lett.* 2015, **161**, 561–564.
8) L. Ding, R. Wei, H. Chen, J. Hu, J. Li, *Appl. Catal. B Environ.* 2015**, 172**, 91–99.
9) X. Gao, X. Zhang, Y. Wang, S. Peng, B. Yue and C. Fan, *Chem. Eng. J.* 2015, **263**, 419–426.
10) T. Li, L. Lin, H. Wei, G. Liang, X. Kuang and T. Liu, *Phys. E: Low-Dimensional Syst. Nanostructures.* 2016, **76**, 198–202.
11) X. Zhang, X. Liu, C. Fan, Y. Wang, W. Yunfang and Z. Liang, *Appl. Catal. B Environ.* 2013**, 132**, 332–341.
12) Y. Wang, Z.Q. Shi, C.M. Fan, X.G. Hao, G.Y. Ding and Y.F. Wang, *Int. J. Miner. Metall. Mater.* 2012, **19**, 467–472.
13) D.H. Wang, G.Q. Gao, Y.W. Zhang, L.S. Zhou, A.W. Xu and W. Chen, *Nanoscale*. 2012, **4**, 7780-7785.
14) G. Nie, X. Lu, W. Wang, M. Chi, Y. Jiang and Ce. Wang, *Mater. Chem. Front.* 2017, **1**, 859-866.
15) W. Hong, L. Wang, K. Liu, X. Han, Y. Zhou, P. Gao, R. Ding and E. Liu, *J. Alloys Compd.* 2018**, 746,** 292-300.
16) Q.X. Xia, N. Shinde, J.M.Yun, T. Zhang, R.S. Mane, Mathur and K.H. Skim, *Electrochim. Acta.* 2018, **271**, 351-360.
17) J. Jiang, K. Zhao, X. Xiao and L. Zhang,. *J. Am. Chem. Soc.* 2012, **134**, 4473-4476.
18) E.M. Doherty, S. De, P.E. Lyons, A. Shmeliov, P.N. Nirmalraj, V. Scardaci. J. Joimel, W.J. Blau, J.J. Boland and J.N. Coleman, *Carbon*. 2009, **47**, 2466-2473.
19) Z.C. Wu, Z.H. Chen, X. Du, J.M. Logan, J. Sippel and M. Nikolou. et al. *Science.* 2004, **305**, 1273–6.
20) K. Zhou, W. Zhou, X. Liu, Y. Sang, S. Ji, W. Li, J. Lu, L. Li, W. Niu, H. Liu and S. Chen, *Nano Energy.* 2015**, *12***, 510-520.
21) H. Wang, H. Yi, X. Chen and X.Wang, *J. Mater. Chem. A* 2014, **2**, 3223-3230.
22) S. Ratha and C. S. Rout, *RSC Adv.* 2015, **5**, 86551-86557.
23) W. G. Fateley, N. T. Mcdecitt and F. F. Bentley, *Appl. Spectrosc.*1971, **25**, 155.
24) V Tian, C. F. Guo, Y. J. Guo, Q. Wang and Q. Liu, *Appl. Surf. Sci.* 2012, **258**, 1949.
25) H. Qi, J. Liu and E. Mader, *Fibers.* 2014, **2**, 295-307.
26) J. Hu, W. Fan, W. Ye, C. Huang and X. Qiu, *Appl. Catal. B Environ.* 2014**, 158**,182–189.

27) H.Y. Jiang, K. Cheng and J. Lin, *Phys. Chem. Chem. Phys.* 2012, **14**, 12114–12121.
28) L. Ye, K. Deng, F. Xu, L. Tian, T. Peng and L. Zan, *Phys. Chem. Chem. Phys.* **2012**, *14*, 82–85.
29) C. Wang, C. Shao, Y. Liu and L. Zhang, *Scr. Mater.* 2008, **59**, 332–335.
30) L. Song, X. Cao, L. Li, Q. Wang, H, Ye, L. Gu, C. Mao, J. Song, S. Zhang and H. Niu, *Adv. Funct. Mater.*, 2017,**27**,1700474.
31) Z. Zhang, Q.C. Zheng and L. Sun, *Ceram Int.* 2017, **43**, 16217-16224.
32) C. Zhu, P. Yang, D. Chao, X. Wang, X. Zhang, S. Chen, B. K. Tay, H. Huang, H. Zhang, W. Mai and H. J. Fan, *Adv. Mater.*, 2015, **27**, 4566–4571
33) Z. Tian, H. Dou, B. Zhang, W. Fan and X. Wang, *Electrochim. Acta.* 2017, **237**, 109–118.
34) I. Moon, S. Yoon and J. Oh, *Chem.Eur. J.*, 2017, **23**, 597–604.
35) D. Zhao, Q. Zhang, W. Chen, X. Yi, S. Liu, Q. Wang, Y. Liu, J. Li, X. Li and H. Yu, *ACS Appl. Mater. Interfaces*, 2017, **9**, 13213–13222.
36) C. Zhu, P. Yang, D. Chao, X. Wang, X. Zhang, S. Chen, B. K. Tay, H. Huang, H. Zhang, W. Mai and H. J. Fan, *Adv. Mater.*, 2015, **27**, 4566–4571.
37) X. Li, K. Liu, Z. Liu, Z. Wang, B. Lia and D. Zhang, *Electrochim. Acta*. 2017, **240**, 43–52.